JOURNAL OF AIRCRAFT
Vol. 30, No. 5, Sept.–Oct. 1993

# Experimental Study of Pylon Cross Sections for a Subsonic Transport Airplane

Dinesh A. Naik*
*ViGYAN, Inc., Hampton, Virginia 23666*
and
Anthony M. Ingraldi† and Odis C. Pendergraft Jr.†
*NASA Langley Research Center, Hampton, Virginia 23681*

**Pylon cross sections that are intended to reduce the installation drag of an underwing propulsive system were investigated on a 1/7 scale low-wing transport model in the NASA Langley 16-ft Transonic Tunnel. The design philosophy for the pylons was to alleviate flow acceleration on the lower surface of the wing without introducing severe adverse pressure gradients near the junction of the pylon and wing. This was achieved by means of a gradually diverging pylon with maximum thickness occurring at the wing trailing edge. The pylon closure occurred aft of the wing trailing edge. A hybrid derivative of this pylon, with a more practical thickness distribution for conventionally mounted engines, also achieved the desired effect. The surface static pressure measurements, surface flow visualization data, and force balance data support the design philosophy.**

## Nomenclature

$b$ = wing span
$C_D$ = drag coefficient, drag/$q_\infty S$
$C_L$ = lift coefficient, lift/$q_\infty S$
$C_p$ = static pressure coefficient, $(p - p_\infty)/q_\infty$
$c$ = local wing chord
$c'$ = local pylon chord (defined to be 0.95 $c$)
$\bar{c}$ = mean aerodynamic chord
$M$ = Mach number
$p$ = static pressure
$q$ = dynamic pressure
$S$ = wing reference area
$x$ = downstream coordinate
$y$ = spanwise coordinate with respect to fuselage centerline
$\eta$ = nondimensional spanwise wing station, $2y/b$

*Subscripts*
min = minimum
$\infty$ = freestream condition

## Introduction

THE aerodynamics of propulsion integration plays a crucial role in the development and marketing of new generation jet transport aircraft. The propulsive assembly typically accounts for 15% of total airplane drag.[1] Reductions in installed drag on the order of 1% of total airplane drag at cruise can translate into substantial financial savings for airline operators, particularly when there is an escalation in the cost of fuel. There are several aspects of propulsion integration that can be addressed in order to reduce the drag penalty associated with the engine installation. Some examples are: nacelle geometry; proximity of the nacelle to the wing; spanwise location of the engine; pylon geometry; and, type of installation (i.e., underwing, overwing, fuselage-mounted). This article examines the effect of the cross-sectional shape of underwing pylons.

The study was a part of an ongoing research effort in transport propulsion integration at NASA Langley Research Center. The propulsion integration is discussed in the context of a 1/7 scale, low-wing transport airplane with underwing pylons (Fig. 1). The airplane has a supercritical wing section and is designed for a cruise lift coefficient of 0.55 at a Mach number of 0.77. Interference effects of underwing, flow-through nacelles with bypass ratios of 6 and 18, with variations in nacelle toe-in and incidence angles, were investigated on this model.[1-3] Computational Fluid analysis (CFD) analysis of the fuselage-wing-pylon-nacelle geometry has also been performed with an Euler code.[4]

The computational results, which are in reasonable agreement with experimental pressure data,[1] indicate high-flow velocities induced on the wing lower-surface by the flow accelerating around the thickest portion of the pylon (Fig. 2). This effect may be compounded by the fact that the pylon maximum thickness occurs near the supercritical wing's maximum thickness. The low pressure on the lower surface of the wing results in a loss of lift. Farther aft, any additional pressure gradients imposed from flow compression as it traverses the pylon trailing-edge closure would be especially undesirable because the supercritical wing section is already designed for an adverse pressure gradient from flow compression due to aft-camber. The result could be flow separation, of the kind shown in Fig. 3, and a consequent increase in drag. The figures

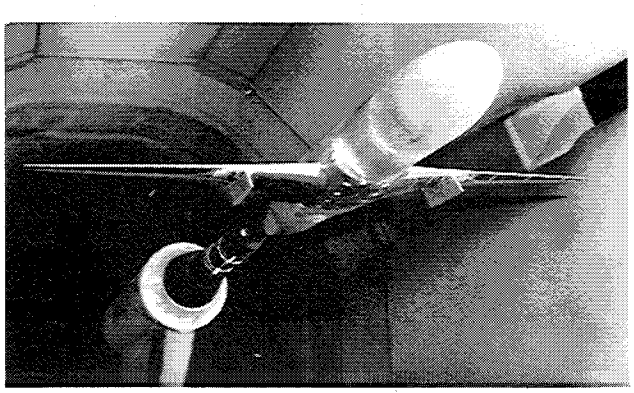

**Fig. 1 Low-wing transport model in the NASA Langley 16-ft Transonic Tunnel. Underwing pylons at $\eta$ = 0.34.**

Presented as Paper 92-0153 at the AIAA 30th Aerospace Sciences Meeting and Exhibit, Reno, NV, Jan. 6–9, 1992; received Feb. 4, 1992; revision received July 20, 1992; accepted for publication July 22, 1992. 

*Research Engineer, 30 Research Drive. Member AIAA.
†Aerospace Engineer, Propulsion Aerodynamics Branch, Applied Aerodynamics Division, M/S 280.

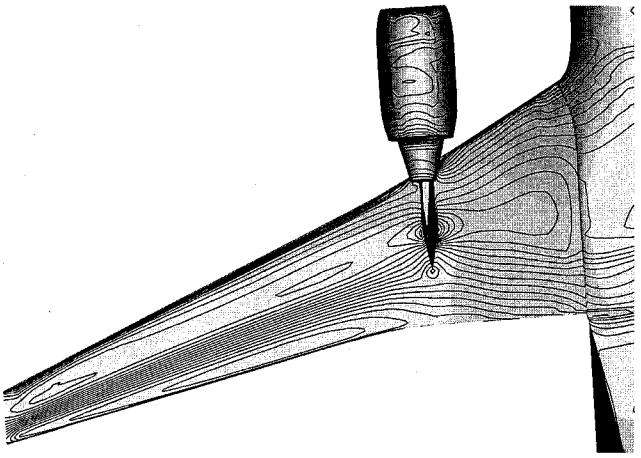

**Fig. 2 $C_p$ contours on wing lower surface from an Euler analysis of the complete airplane with installed pylon and nacelle at $\eta = 0.34$. $M_\infty = 0.77$, $C_L \approx 0.55$.[4]**

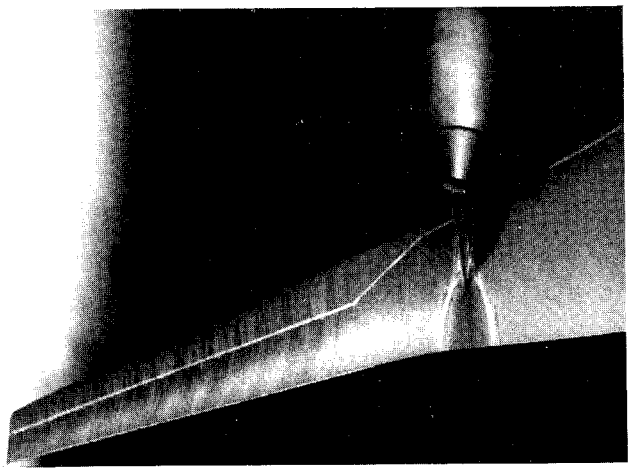

**Fig. 3 Wing lower surface oil flow visualization photograph for pylon-nacelle installed at $\eta = 0.34$. $M_\infty = 0.77$, $C_L \approx 0.55$.[4]**

confirm that a partial-chord pylon can have a significant local effect on the wing flow near the junction.

It has been hypothesized that the airflow problems on the lower surface of the wing could be avoided with a flat-sided pylon of increasing thickness whose closure is moved aft of the wing trailing edge, while maintaining the pylon maximum thickness. In order to achieve maximum effect, the pylon is widest at the wing trailing edge.[5] This type of pylon is called a compression pylon. The compression pylon would be expected to have higher skin friction drag than a conventional partial-chord pylon because of the larger wetted area. However, at cruise, this could be more than offset by lower interference drag.

References 5 and 6 showed the usefulness of the compression pylon concept for a high-wing transport aircraft where any airflow problems in the channel between the pylon and the fuselage are particularly amenable to pylon shaping. The present study examines the compression pylon idea in the context of the more prevalent low-wing transport configuration.

The design could be further refined by varying the toe-in angle (earlier pylon-nacelle studies[3] showed that the effect of changes in pylon toe-in angle, though for the most part minimal, can sometimes result in lower installation drag), and also by tailoring the outboard side of the pylon differently from the inboard side to accommodate any crossflow arising from wing sweep and fuselage blockage. This latter shape is referred to as the hybrid pylon in this article.

The current investigation compares the installation effect of three pylon designs vs the clean wing in terms of the wing surface pressure coefficient distributions, the amount of flow separation at the pylon-wing junction, and the aerodynamic force characteristics of the transport model.

## Apparatus and Procedure

The NASA Langley 16-ft (4.88 m) Transonic Tunnel is a single-return, continuous-flow, atmospheric wind tunnel with a test section of octagonal cross section and a throat area of 199.15 ft$^2$ (18.5 m$^2$). The model was sting-mounted and held near the test section centerline at all angles of attack by the support-system arrangement.

The airplane model is a $\frac{1}{17}$ scale representation of a 150-passenger, twin-engine transport designed to cruise at $M_\infty = 0.77$ and $C_L = 0.55$. Overall wing dimensions are given in Table 1. The supercritical wing coordinates and other model details may be obtained from Ref. 1.

Three pylon cross sections were studied. These were the NASA SC(2)-0012, the compression, and the hybrid cross sections (see Fig. 4a). The SC(2)-0012 airfoil was specifically tailored[7] for transonic flow regimes in an attempt to improve upon the performance of a conventional NACA 0012 airfoil. The pylons were notched back 5% from the wing leading edge as shown in Fig. 4b. The SC(2)-0012 pylon terminated at the wing trailing edge. For all pylons, the maximum thickness was defined relative to the local SC(2)-0012 pylon chord.

The compression and the hybrid pylons extended beyond the wing trailing edge but had approximately the same maximum thickness as the SC(2)-0012 pylon. The compression pylon coordinates are available in Ref. 5. The hybrid pylon, with an inboard compression side and an outboard SC(2)-0012 side was expected to provide a compromise wing pressure distribution that is closest to that of the clean wing.[6] The compression pylon has a rather awkward thickness distribution from a structural load-bearing standpoint for a conventionally mounted engine. In this context, the hybrid shape is a more practical design. The compression pylon would be better suited to an engine mounted near the wing trailing edge. An aft-underwing mounted engine can result in an increase in lift and lower installed drag.[8,9]

**Table 1. Overall model wing dimensions[3]**

| | | |
|---|---|---|
| $S$ | 587.96 sq. in. | 0.3793 m$^2$ |
| Aspect ratio | 10.795 | |
| Taper ratio | 0.275 | |
| $\frac{1}{4}$ chord sweep | 21 deg | |
| $\frac{1}{4}$ chord dihedral | 5.78 deg | |
| $\bar{c}$ | 8.176 in. | 0.2077 m |

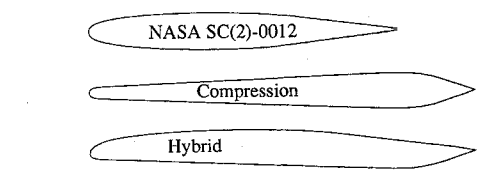


**a) Cross section**

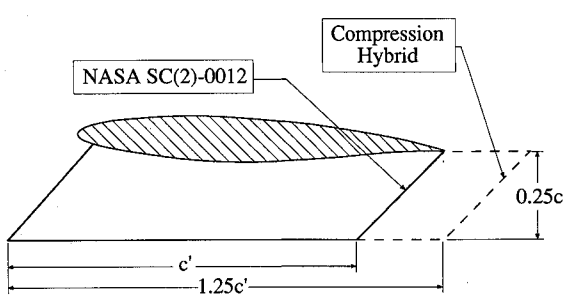


**b) Size**

**Fig. 4 Pylon geometry.**

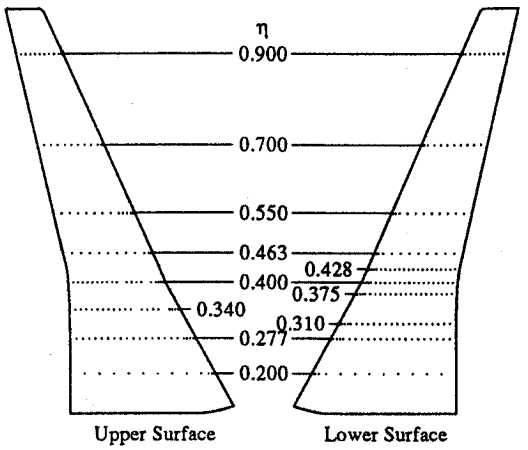


**Fig. 5 Wing surface pressure orifices.[2]**

Two sets of pylons were constructed. One set of three pairs was sized with respect to the local wing chord for installation at the $\eta = 0.340$ wing locations. The other set was sized for installation at the $\eta = 0.400$ wing locations. $\eta = 0.400$ is a possible alternative location for a higher bypass ratio engine that might not have sufficient ground clearance at $\eta = 0.340$. The photograph of Fig. 1 shows pylons at $\eta = 0.340$.

Forces and moments were obtained on the completely metric model from an internal six-component strain-gauge balance. More than 300 wing surface pressure orifices were located on the port wing. The spanwise locations of each orifice row are shown in Fig. 5. The orifices on the lower surface were concentrated in the vicinity of the pylon installation locations of $\eta = 0.340$ and $\eta = 0.400$ so that local flow phenomena around the pylons could be examined in greater detail. Further details of this instrumentation can be found in Ref. 1. The data reduction procedure is described in Ref. 10.

The pylons were not instrumented. A fluorescent oil flow technique was employed to obtain flow visualization on the wing in the vicinity of the pylons to determine the extent of flow separation in this region. Transition grit was fixed on the model based on the observations from oil flow studies.[1]

Four different pylon toe-in angles (0, 1, 2, and 3 deg) were investigated for each pylon tested. Toe-in angles greater than 3 deg were deemed impractical and were not investigated. Toe-out angles were not studied because spanwise flow was expected on the wing.

It is difficult to ascertain precisely the individual contributions of the pylon drag components (skin-friction drag, induced drag, wake drag, and wave drag). However, general inferences regarding installation drag will be made from the pressure, flow visualization, and force data. It must be reiterated that any conclusions drawn only from the drag polars must be tempered by two concerns: 1) the pylon bottom is flat; and 2) the trailing edge closures for the two "long" pylons were not derived from a design process for minimum wake drag.

## Results

The effect of toe-in angle was found to be minimal at cruise. The discussions are mainly focused on the following pylon/optimum-toe-in combinations: SC(2)-0012 at 1 deg, compression at 3 deg, and hybrid at 2 deg.

### Effect of Pylon Cross-Sectional Shape at $\eta = 0.340$

The adjacent ($\eta = 0.310$ and $\eta = 0.375$) lower-wing $C_p$ distributions for the $\eta = 0.34$ pylons at optimum toe-in angle are compared with the clean wing, for $M_\infty = 0.77$ and $C_L \approx 0.55$, in Fig. 6. The wing pressures for the other orifices are not shown because the effect was found to be quite local.

The NASA SC(2)-0012 pylon is seen to induce high negative $C_p$ on the inboard lower surface of the wing. The two pylons

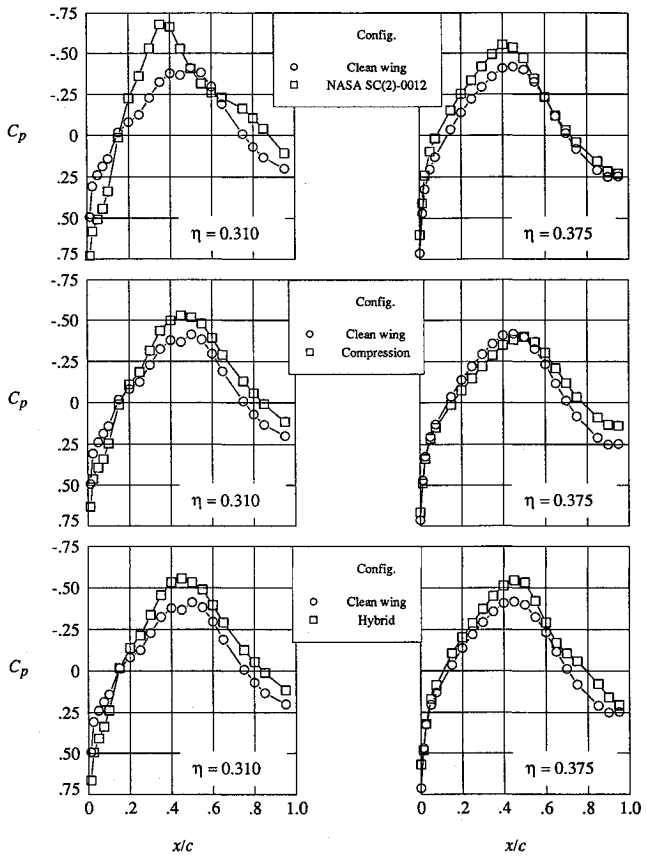


**Fig. 6 Wing lower surface $C_p$ at $\eta = 0.310$ and $\eta = 0.375$. Pylons at $\eta = 0.34$ vs the clean wing. $C_L \approx 0.55$, $M_\infty = 0.77$.**

that are flat on the inboard side were found to induce less negative $C_p$ peaks than the peak induced by the SC(2)-0012 pylon. The compression and hybrid pylon installations result in pressure distributions that are closer to the clean wing.

Between 0.4 and 0.6 $x/c$, the SC(2)-0012 pylon induces a stronger adverse pressure gradient on the inboard wing lower surface than do the flat-sided pylons. However, farther aft, on the wing lower surface between 0.6 $x/c$ and 0.8 $x/c$ and at $\eta = 0.310$, the SC(2)-0012 pylon appears to induce a lower adverse pressure gradient. This gentler gradient seems to be in direct contradiction to the design philosophy of the compression pylon, but can be explained with the flow visualization photographs shown in Fig. 7.

The SC(2)-0012 pylon is seen to cause a larger separated flow region on the inboard side of the wing than does the compression pylon. The $\eta = 0.310$ row of wing orifices (Fig. 5) partially traverses the outer reaches of the separated flow region associated with the SC(2)-0012 pylon (Fig. 7a). This same orifice row does not traverse the separated flow region associated with the compression pylon (Fig. 7b). The pressure variation within the separated flow region could be expected to be more gradual than the pressure gradient outside it.

The drag polars for the pylon installations and for the clean wing are shown in Fig. 8. Figure 9 is an enlargement around the cruise condition. Drag data interpolated to $C_L = 0.55$ is given in Table 2. The compression and hybrid pylons outperform the SC(2)-0012 pylon at the design cruise $C_L$ and over most of the lift range.

Figures 6–9 show that the compression pylon concept, which earlier has proven useful for alleviating flow accelerations in the channel between the pylon and fuselage of a high-wing aircraft,[5] also works well for a low-wing aircraft, primarily because it does not impose strong pressure gradients on the wing.

There is a large divergence between drag polars at the lower off-design lift conditions. In particular, $C_{D\min}$ is approximately

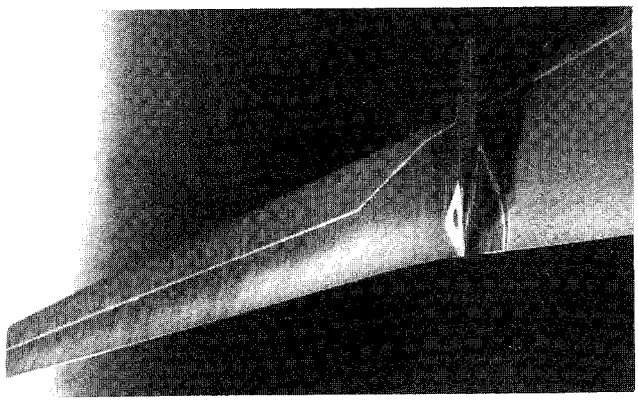

a) SC(2)-0012 pylon

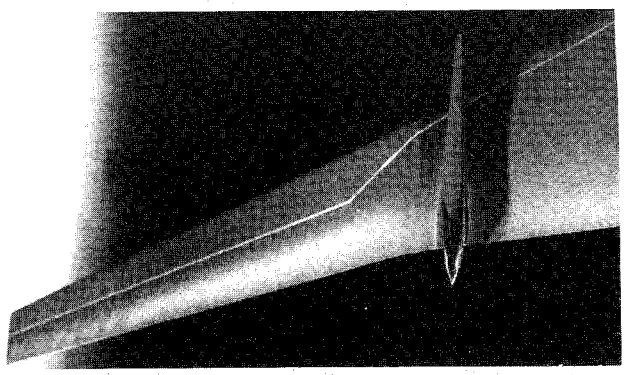

b) Compression pylon

**Fig. 7 Wing lower surface oil flow visualization for pylons at $\eta$ = 0.34, $M_\infty$ = 0.77, $C_L \approx$ 0.55.**

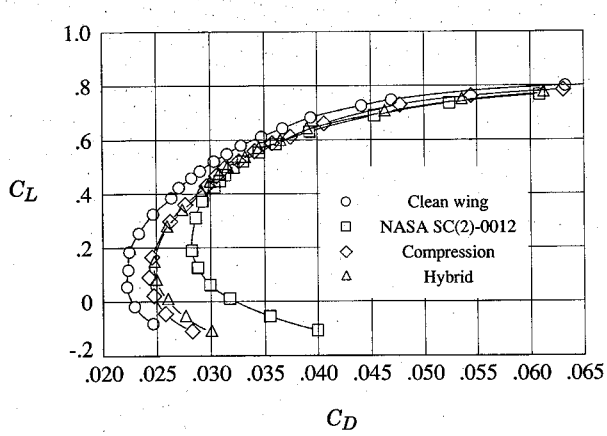


**Fig. 8 Airplane drag polars. Pylons at $\eta$ = 0.34 vs clean wing. $M_\infty$ = 0.77.**

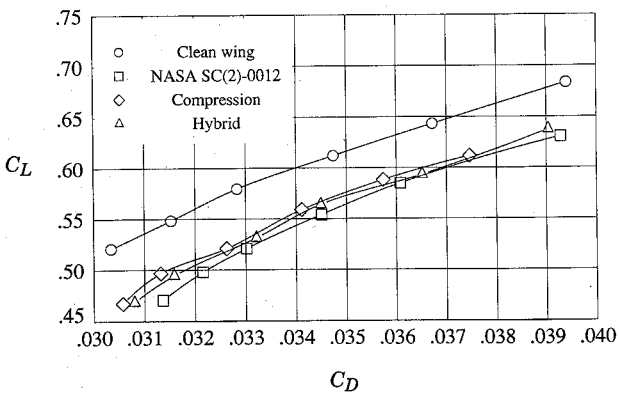


**Fig. 9 Enlargement of drag polars near $C_L \approx$ 0.55. Pylons at $\eta$ = 0.34, $M_\infty$ = 0.77.**

**Table 2 Airplane $C_D$ at $C_L$ = 0.55, $M_\infty$ = 0.77; pylons at $\eta$ = 0.340**

| Pylon | $C_D$ |
|---|---|
| Clean wing | 0.0316 |
| SC(2)-0012 | 0.0343 |
| Compression | 0.0337 |
| Hybrid | 0.0339 |

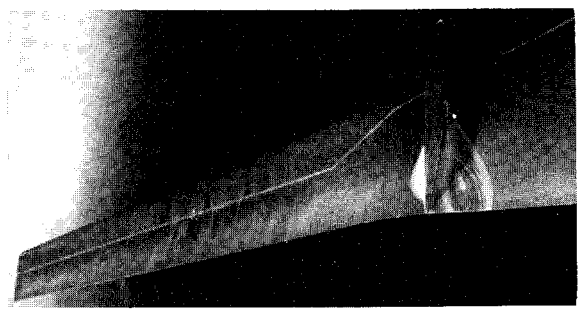

a) SC(2)-0012 pylon

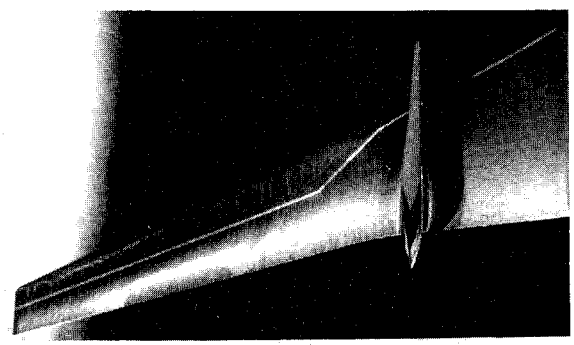

b) Compression pylon

**Fig. 10 Wing lower surface oil flow visualization for pylons at $\eta$ = 0.34, $M_\infty$ = 0.77, at $C_{D\min}$.**

0.003–0.004 higher for the SC(2)-0012 pylon. While the compression and hybrid pylons would be expected to have higher skin-friction drag than the SC(2)-0012 pylon, the higher $C_{D\min}$ for the SC(2)-0012 pylon can be attributed to flow separation. The surface oil flow for the SC(2)-0012 pylon at $C_{D\min}$ (Fig. 10a) shows the large region of separated flow at the pylon-wing junction, while the compression pylon shows minimal separation (Fig. 10b) for its $C_{D\min}$.

Figures 7a and 10a indicate that the amount of flow separation on the outboard side of the SC(2)-0012 pylon is less than on the inboard side. This is a consequence of the spanwise crossflow being interrupted by the pylon. The asymmetry, shown in Fig. 6, between the inboard and outboard pressure distributions can also be attributed to this crossflow effect.

Depending on local flow angularity, on the inboard side the crossflow could have either energized the separated flow or resulted in an even steeper adverse pressure gradient. [Numerical solutions from an Euler code[4] had shown (Fig. 2) steeper inboard gradients for a partial chord pylon.] The latter seems to have occurred with the SC(2)-0012 pylon.

Figures 10a and 7a also show that the amount of inboard flow separation, due to the SC(2)-0012 pylon installation, is much more at the $C_{D\min}$ condition than at cruise. This is because higher flow velocities and consequently, higher aft-compression gradients, are present on the wing lower surface at negative angles of attack.

### Effect of Pylon Cross-Sectional Shape at $\eta$ = 0.400

Figure 11 shows the drag polars for the pylons located at $\eta$ = 0.40. At this outboard location, the compression and hybrid pylons had lower overall drag than the SC(2)-0012

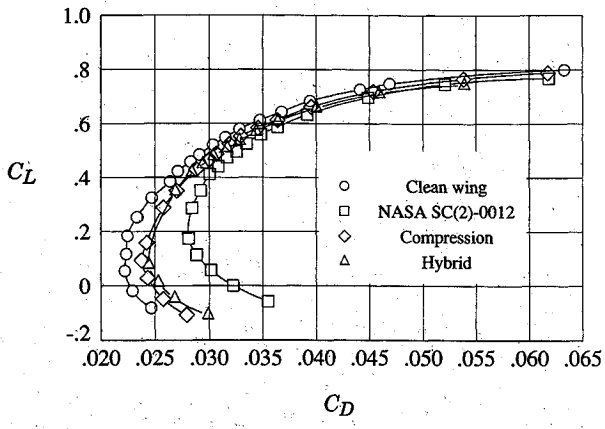


**Fig. 11 Airplane drag polars. Pylons at $\eta = 0.40$ vs clean wing. $M_\infty = 0.77$.**

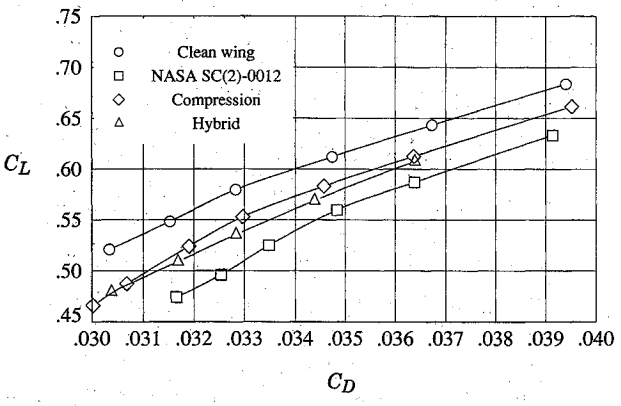


**Fig. 12 Enlargement of drag polars near $C_L \approx 0.55$. Pylons at $\eta = 0.40$, $M_\infty = 0.77$.**

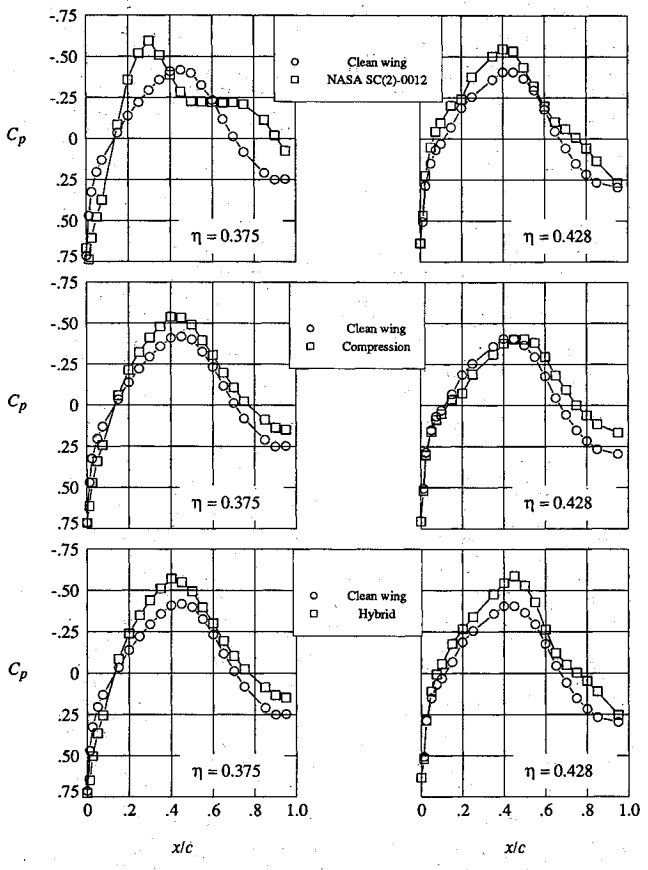


**Fig. 13 Wing lower surface $C_p$ at $\eta = 0.375$ and $\eta = 0.428$. Pylons at $\eta = 0.40$ vs the clean wing. $C_L \approx 0.55$, $M_\infty = 0.77$.**

**Table 3 Airplane $C_D$ at $C_L = 0.55$, $M_\infty = 0.77$; pylons at $\eta = 0.400$**

| Pylon | $C_D$ |
|---|---|
| Clean wing | 0.0316 |
| SC(2)-0012 | 0.0344 |
| Compression | 0.0328 |
| Hybrid | 0.0335 |

pylon. This is consistent with the results obtained at the inboard ($\eta = 0.34$) location. The enlargement around cruise is shown in Fig. 12 and interpolated drag coefficients for $C_L = 0.55$ are shown in Table 3. The compression pylon resulted in the lowest airplane drag at cruise, roughly 5% lower than that for the SC(2)-0012 pylon.

Figure 13 shows the adjacent ($\eta = 0.375$ and $\eta = 0.428$) lower-wing pressures. The same trends are observed. The inboard row is close enough to the pylon location for the $C_p$ distribution to reflect the separation associated with the SC(2)-0012 pylon.

## Conclusions and Recommendations

Pylon cross sections were investigated on a $\frac{1}{17}$ scale low-wing transport model in the NASA Langley 16-ft Transonic Tunnel. A compression pylon and its hybrid derivative seem promising from the standpoint of lower drag for propulsion integration.

The basic approach was to alleviate flow acceleration without introducing severe adverse pressure gradients near the pylon-wing junction. The flow acceleration is reduced by means of a gradually diverging pylon with maximum thickness at the wing trailing edge. The pylon trailing-edge closure (flow compression region) occurs aft of the wing trailing edge. The resulting wing pressure distributions are close to those for the clean wing; implying small loss of lift and also minimal flow separation at the pylon-wing junction.

Although this study of generic pylon cross sections has indicated some useful performance trends, the following issues should be investigated:

1) The compression pylon, with its bulkier aft end and thinner forward end poses a structural challenge for conventionally mounted forward engines. This is not as crucial for the hybrid pylon because it has a more uniform thickness distribution.

2) This study has shown that the nature and extent of the separated flow at the pylon-wing junction is a crucial determinant of installation drag. However, high Reynolds number studies are needed because this kind of pressure-gradient-induced separation could be quite different at full-scale Reynolds number.

3) The compression and hybrid pylon concepts should be tested with a nacelle attached because the presence of a nacelle could, depending on proximity, further compound or alleviate flow accelerations and gradients near the pylon-wing junction.

4) For nacelles very close to the wing and for very high bypass ratio nacelles, the effect of the fan/jet exhaust should be considered.

5) Three-dimensional inverse-design methods should be used to design pylon and fillet geometry from prescribed pressure distributions.

6) A pylon geometry might only be good at a single design point, whereas practical implementation could require geometry optimization for multipoint design.

## Acknowledgments

This research was funded by the National Aeronautics and Space Administration under NASA Contract NAS1-17919 while D. A. Naik was in residence at ViGYAN, Inc. The authors would like to thank J. Claude Patterson Jr., formerly of NASA Langley, who proposed the compression pylon concept.

## References

[1]Pendergraft, O. C., Jr., Ingraldi, A. M., Re, R. J., and Kariya, T. T., "Installation Effects of Wing-Mounted Turbofan Nacelle/Pylons on a 1/17th-Scale, Twin-Engine, Low-Wing Transport Model," NASA TP 3168, March 1992.

[2]Ingraldi, A. M., Kariya, T. T., Re, R. J., and Pendergraft, O. C., Jr., "Interference Effects of Very High Bypass Ratio Nacelle Installations on a Low-Wing Transport," American Society of Mechanical Engineers 91-GT-241, June 1991.

[3]Pendergraft, O. C., Jr., Ingraldi, A. M., Re, R. J., and Kariya, T. T., "Nacelle/Pylon Interference Study on a 1/17th-Scale, Twin-Engine, Low-Wing Transport Model," AIAA Paper 89-2480, July 1989.

[4]Naik, D. A., Chen, H. C., Su, T. Y., and Kao, T. J., "Euler Analysis of Turbofan/Superfan Integration for a Transport Aircraft," AGARD 69th Fluid Dynamics Panel Meeting and Symposium on Engine-Airframe Integration for High Performance Aircraft and Missiles, Fort Worth, TX, Oct. 7–10, 1991.

[5]Carlson, J. R., and Lamb, M., "Integration Effects of Pylon Geometry on a High-Wing Transport Airplane," NASA TP 2877, Feb. 1989.

[6]Naik, D. A., "Innovative Pylon Concepts for Engine-Airframe Integration for Transonic Transports," AIAA Paper 89-1819, June 1989.

[7]Mineck, R. E., and Lawing, P. L., "High Reynolds Number Tests of the NASA SC(2)-0012 Airfoil in the Langley 0.3 m Transonic Cryogenic Tunnel," NASA TM 89102, July 1987.

[8]Abeyounis, W. K., and Patterson, J. C., Jr., "Effect of Location of Aft-Mounted Nacelles on Longitudinal Aerodynamic Characteristics of a High-Wing Transport Airplane," NASA TP 3047, Dec. 1990.

[9]Abeyounis, W. K., and Patterson, J. C., Jr., "Effect of Underwing Aft-Mounted Nacelles on the Longitudinal Aerodynamic Characteristics of a High-Wing Transport Airplane," NASA TP 2447, Dec. 1985.

[10]Mercer, C. E., Berrier, B. L., Capone, F. J., Grayston, A. M., and Sherman, C.D., "Computations for the 16-Foot Transonic Tunnel," NASA TM 86319, Jan. 1987.